Received: 14 February 2024 | Revised: 16 May 2024 | Accepted: 27 July 2024

DOI: 10.1111/ffe.14411

ORIGINAL ARTICLE

FFEMS Fatigue & Fracture of Engineering Materials & Structures WILEY

Low cycle fatigue behavior of AZ31 magnesium alloy joined by friction stir welding

Murat Türkan[1,2] | **Özler Karakaş**[2] | **Filippo Berto**[3]

[1]Department of Mechanical Engineering, Faculty of Engineering, Izmir University of Economics, Izmir, Turkey

[2]Department of Mechanical Engineering, Faculty of Engineering, Pamukkale University, Denizli, Turkey

[3]Department of Chemical Engineering, Materials and Environment, Sapienza University of Rome, Rome, Italy

Correspondence
Özler Karakaş, Department of Mechanical Engineering, Faculty of Engineering, Pamukkale University, Kinikli, 20160, Denizli, Turkey.
Email: okarakas@pau.edu.tr

Funding information
Scientific Research Coordination Unit of Pamukkale University, Grant/Award Number: 2019FEBE039

Abstract

This study, aims to weld the 5.2 mm thick AZ31 magnesium alloy with conventional friction stir welding at the highest joining efficiency. As a result of the experiments, 88% joining efficiency in tensile strength has been obtained at 1250 rpm, 400 mm.min^{-1} welding parameter. As a result of micro–macrostructure photographic examinations of the samples joined with these parameters, it is seen that the joining is fully realized. Samples joined with these parameters have been used in fatigue tests. According to the strain-controlled low cycle fatigue test results performed on welded and base metal samples, the base metal samples have exceeded the 50,000-cycle limit without failure, with an elongation rate of 0.3%, and the welded samples with an elongation rate of 0.2%. Low cycle fatigue parameters of welded and base metal samples have been obtained according to the Coffin-Manson-Basquin equation.

KEYWORDS
conventional friction stir welding, low cycle fatigue, magnesium alloys

Highlights

- In joining AZ31 alloy with FSW, a high joining efficiency of 88% was achieved.
- Similar fatigue test results showed that the weld quality was retained along the joint.
- Coffin-Manson-Basquin equation constants were determined.

1 | INTRODUCTION

Magnesium alloys offer a unique combination of properties such as lightness, strength, and rigidity when used as materials for manufactured parts. Magnesium alloys, with a density of 1.74 g/cm^3, are approximately 80% and 35% lighter than steel (7.86 g/cm^3) and aluminum alloys (2.7 g/cm^3), respectively.[1] It is also the lightest of the structural metals.[2,3] Magnesium alloys rank third in use as structural parts after steel and aluminum.[4]

Magnesium alloys with high strength-to-weight ratios have significant potential for energy savings in the automotive and aerospace industries.[5–9] Magnesium alloys have higher strength, hardness, thermal stability, and thermal conductivity than plastic. They also have higher specific strength, flexibility, and impact resistance than

aluminum alloys.[10] Additionally, magnesium alloys offer excellent vibration-damping properties and heat dissipation properties, which is an important factor for the automotive and aerospace industries.[11]

There are studies in the literature indicating that pores occur in the weld metal when joining magnesium alloys with traditional fusion welding techniques. These pores negatively affect the mechanical properties of the joints.[12–17] In addition, the high expansion coefficient of magnesium alloys causes large deformation-distortion of the welded part.[18] Magnesium alloys can be joined by a wide variety of welding techniques, but various disadvantages such as wide heat-affected zone, alloying element loss, high residual stresses, and cracks have been reported to occur when using conventional methods.[19–22]

Friction stir welding (FSW) process, which is a solid-state welding technique, includes the consideration of temperature, mechanics, metallurgy, and interactions,[23] and is a revolutionary welding technique in terms of energy efficiency, environmental friendliness, and seam quality. The advantages of the FSW process include achieving good strength, toughness, and minimal distortion in welded parts when joining magnesium alloys and other light metals.[24] In the traditional FSW process, a tool consisting of a pin and shoulder, rotating around its own axis and able to maintain its mechanical properties at high temperatures is used. The tool plunges into the materials by rotating to be welded and moves forward by rotating along the welding direction.[25] In this process, the base material does not melt and the heat required for welding is provided by the friction between the tool and the workpiece and the plastic deformation of the base material.[26,27] The side in the workpiece where the tool rotation direction is the same as the welding direction is called the advancing side (AS), and the side where the tool rotation direction is opposite to the welding direction is called the retreating side (RS).[28] As the tool rotating moves in the welding direction, the material moves from AS to RS and solid-state joining occurs.[29] The absence of melting in this welding method prevents defects caused by melting and solidification, which are frequently encountered in the welding of magnesium alloys.[30] Uncontrolled melting-solidification and high heat input cause problems in the welding of magnesium alloys. For this reason, the FSW process, which is a thermomechanical process in which melting does not occur with low heat input, is a strong alternative in joining magnesium alloys.

Applications using magnesium alloys inevitably involve welded manufacturing. Since welded manufacturing generally causes a decrease in the strength of materials due to microstructural changes and/or potential welding defects along the weld, examining the behavior of welded joints, especially under cyclic loads, is very important to prevent major damage in structural parts.[31,32] In addition, Marsavina et al[33] have stated that obtaining some correlations between fatigue strength, tensile strength, and hardness will be useful for designers and manufacturers to predict the durability of components. A commonly used classification in examining the fatigue behavior of metals is based on fatigue life. In high cycle fatigue tests, the applied stress is low enough to create elastic deformation in the material, but plastic deformation may occur at the crack tip. In low cycle fatigue tests, plastic deformation is more effective.

In this study, the low cycle fatigue behavior of welded and base metal AZ31 magnesium alloy was investigated. Welding operations were carried out with a conventional FSW process. The micro–macrostructure and hardness distribution of the samples joined at 1250 rpm, 400 mm. min^{-1} welding parameters, where 88% joining efficiency was achieved according to tensile strength, were examined to determine the structure of the welding region. As a result of these examinations, it was understood that the joining is defect-free, therefore welded samples joined at this parameter were used in fatigue tests. Strain-controlled low cycle fatigue tests were carried out on both welded and base metal samples at 10 Hz with six different strain values (0.2%, 0.3%, 0.35% 0.4%, 0.5%, 0.6%) and three samples at each strain value. In addition, since low cycle fatigue test data can be represented by the Coffin-Manson-Basquin equation, the constants of this equation were obtained for both welded and base metal samples.

2 | MATERIALS AND WELDING TECHNOLOGY

AZ31 magnesium alloy sheets with a thickness of 5.2 mm and dimensions of 600 × 900 mm were commercially obtained for the experiments. The chemical composition of the supplied AZ31 magnesium sheets is shown in Table 1.

The FSW process was carried out on a conventional semi-automatic milling machine. Mold design and production were carried out to fix the workpieces during the FSW process. This mold consists of three parts. These parts were obtained by laser cutting from S420 quality steel. Dimensional stability was achieved by removing burrs from the surface by milling and grinding after laser cutting. In addition, the materials to be welded were cut into 100 × 200 mm dimensions with a water jet, as tightly as possible from the side surfaces of the mold. In this way, the movement of the material to be welded was prevented by the mold side surfaces. Vertical movement of the workpieces during welding was prevented by clamps. A photograph of the assembled material holding

TABLE 1 Chemical composition of AZ31 magnesium alloy (% weight).

Alloy	Al	Si	Zn	Fe	Mn	Cu	Ni	Mg
AZ31	2.5–3.5	≤0.30	0.7–1.3	≤0.005	≥0.2	≤0.05	≤0.005	balance

mold at the end of a welding process is shown in Figure 1.

Tool pin geometry is important during the FSW process as intense material flow occurs. Tool pin geometry directly affects the mechanical properties of the joints. Chauhan and Kumar[34] have stated that the joints using the threaded pin among cylindrical, tapered, and threaded pin profiles have shown the best impact strength due to better stirring. Similarly, Rajakumar et al[35] have obtained the best tensile strength values from samples joined with threaded cylindrical pin profiles in their study made with AZ61A alloy. Patel et al[36] in their study with AZ91 alloy, the highest tensile strength was obtained from the tool with threaded straight cylindrical pin among threaded straight cylindrical pin, tapper cylindrical pin, and straight cylindrical pin. Similarly, Singh et al[37] in their study on the ZE41 alloy obtained better results with threaded cylindrical pin geometry than with straight cylindrical pin geometry. It can be said that the presence of thread in the pin geometry facilitates the vertical movement of the material. For this reason, a tool with a cylindrical threaded pin was used. Tools with M5 threaded pins with a shoulder diameter of 21 mm and a pin length of 5 mm were produced by machining. The dimensions of the produced tools are shown in Figure 2. During the FSW process, high temperatures are reached and the tool must be able to maintain its mechanical properties at these high temperatures. For this reason, X40CrMoV5–1 (H13) hot work tool steel was chosen as the tool material. In this steel, molybdenum and vanadium are used to increase strength. Chromium content helps increase its resistance to softening when used at high temperatures. This type of steel offers a very good combination of impact and wear resistance by heat treatment and has good hardness at red heat. Additionally, this type of steel is resistant to rapid cooling. The tool material in cylindrical section without heat treatment was brought to its final dimensions with a CNC lathe. After machining, the heat treatment was done in a professional heat treatment factory. After heat treatment, a hardness of 54 HRC was achieved on the outer surface of tool. No wear or breakage occurred in the tools during the experiments.

Another significant welding parameter is the tool tilt angle relative to the workpiece surface and plunge depth. A suitable tool tilt angle, which is reverse direction to the direction of feed, enables the tool shoulder to hold the material stirred with the pin and to direct effectively

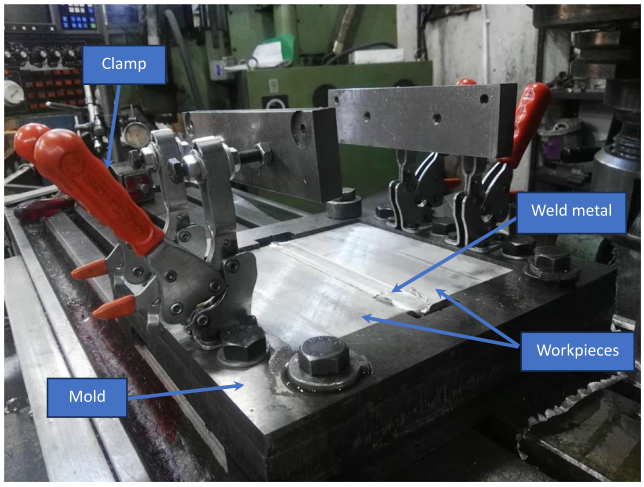

FIGURE 1 Material holder mold. [Colour figure can be viewed at wileyonlinelibrary.com]

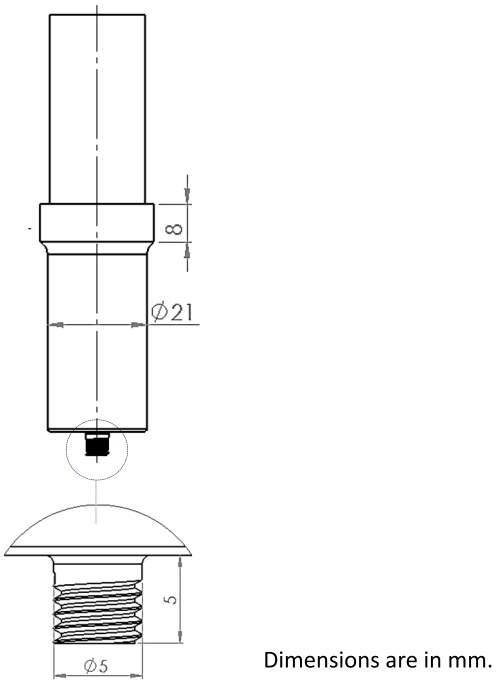

FIGURE 2 Tool geometry. [Colour figure can be viewed at wileyonlinelibrary.com]

the stirred material.[18,38,39] Zhang et al[40] stated that the tool tilt angle must be between 1–3° to make properly FSW. Tool tilt angle directly affects the joining quality and defect formation. Long et al[41] have studied the effect of tool angle on weld properties in FSW with the finite element method. Wormhole defects have occurred when

the tool tilt angle is 0°, whereas these defects have not occurred when the tilt angle is 2°. In their study to improve the surface properties of the cast ZK60 alloy, Vigneshkumar et al[42] stated the most appropriate tool angle is 2° (range 0°–4°). This situation is related to the optimization of heat generation and material flow at a 2° tilt angle. Moreover, the tilt angle is 2° in a study in which 100.8% joint efficiency is obtained.[43] In a study with AZ31[44] tool tilt angle is 2.5°. Optimization of heat generation, material flow, grain boundary strengthening, and homogeneous particle distribution is achieved with the 2° tool tilt angle. Therefore, 2° was used for the tool tilt angle in all experiments.

The plunge depth of the pin in the workpiece is another significant process parameter. Plunge depth has a significant impact on tensile strength and notch impact energy.[45] The depth of the plunge is directly dependent on the pin length. In addition, the shoulder surface of the tool must be in constant contact with the surface of the workpiece in order to effectively move the mixed material during FSW. In two different studies where three different values for the plunge depth (0.03 mm, 0.12 mm, and 0.21 mm) were used, the best mechanical properties were obtained at the plunge depth of 0.12 mm.[46,47] When the plunge depth is low, the tool shoulder cannot make sufficient vertical pressure. In the opposite case, when the plunge depth increases too much, local thinning occurs. Additionally, defects may occur due to increased heat input. As a result, when the studies in the literature are examined, it is understood that it is appropriate to use a tool penetration depth of approximately 0.15 mm to ensure an effective joining with FSW. Therefore, 0.15 mm plunge depth was used in all experiments.

Pre-welding experiments were carried out with many welding parameters. Based on these pre-welding experiments, it was understood that the ratio of the tool rotation speed to the tool feed speed should be between 2 and 3 with a 21 mm shoulder diameter tool. With a 21 mm shoulder diameter tool, 1,250 rpm, 400 mm/min^{-1} parameter was determined as the most suitable parameter. In order to determine this most suitable welding parameter for fatigue tests, a parameter analysis was carried out with reference to tensile tests.

3 | METHOD

Tensile test samples were obtained by laser cutting. Base metal and welded tensile test specimens were produced in the same dimensions, according to EN ISO 6892-1 and EN ISO 4136 standards, respectively. The dimensions of the tensile test samples are shown in Figure 3. Tensile

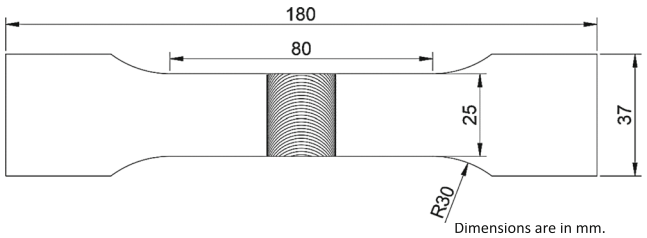

FIGURE 3 Tensile test sample dimensions.[1]

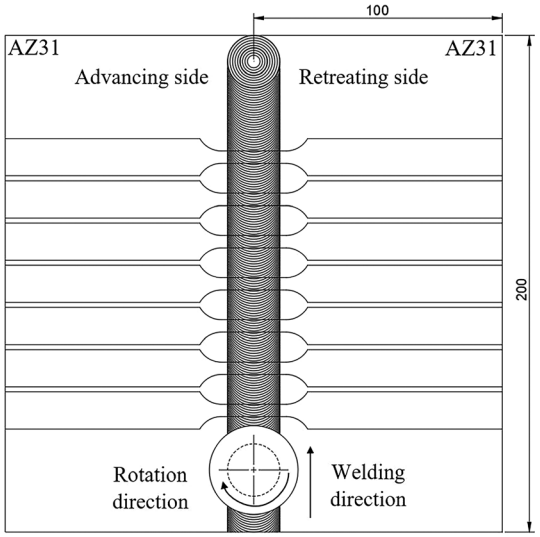

FIGURE 4 Exact positions of fatigue test specimens removed from a welded plate.[1]

tests were carried out on the MTS CRITERION (Model 45) brand universal tensile test device.

ISO 12106:2017 (metallic materials - fatigue testing - axial-strain-controlled method) standard is used to determine the fatigue behavior of uniaxial samples under strain control at constant amplitude, constant temperature, and constant strain rates, including $R_\varepsilon = -1$. Here it is defined as $R_\varepsilon = \varepsilon_{min}/\varepsilon_{max}$. Depending on this standard, fatigue test samples from welded and base metal plates were obtained by wire erosion machine. In fatigue test samples, the wire erosion method was preferred so that the cutting process did not affect the mechanical properties of the samples. Seven fatigue test specimens were removed from each welded plate. The exact removal locations of these samples from the welded parts are shown in Figure 4. Since the lengths of these samples were too long for the working range of the device where the fatigue test was performed, the samples were shortened by machining. The final dimensions of the fatigue test samples are shown in Figure 5 and their photographs are shown in Figure 6.

Fatigue tests were carried out on a SHIMADZU (EHF-LV020K2–020) brand fatigue test device. Strain-controlled low cycle fatigue tests were performed on both welded and base metal samples at 10 Hz, with six different strain values (0.2%, 0.3%, 0.35% 0.4%, 0.5%, 0.6%) and three samples at each strain value.

Micro–macrostructure and hardness examinations were carried out to determine the structure of the weld area. For micro–macrostructure and hardness examinations, cross-sectional samples were taken from the welding area by machining. Micro-macrostructure samples were sanded from coarse to fine and then polished using felt with diamond dust suspension poured on them. To reveal the microstructure of the welded joints, the polished samples were etched with a solution using 5 ml acetic acid, 6 g picric acid, 10 ml water, 100 ml ethanol until a brown film was formed on the sample surface. Microstructure photographs were taken from the stir zone (SZ), thermomechanical affected zone (TMAZ), heat affected zone (HAZ), and base material (BM) through an optical microscope with 20 times and 200 times magnification. The macrostructure photograph was taken at five times magnification.

Microhardness examinations were carried out by applying a 500 g load for 10 s at 2 mm intervals on a polished sample taken from the cross-section of the welded part. Microhardness measurement points along the cross section are shown schematically in Figure 7.

In addition, the welded samples damaged as a result of the fatigue test were examined with a scanning electron microscope (SEM) to better understand the cause of the failure.

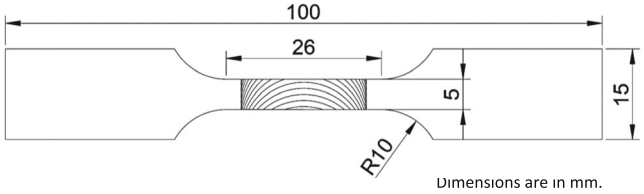

FIGURE 5 Final dimensions of the fatigue test sample.[1]

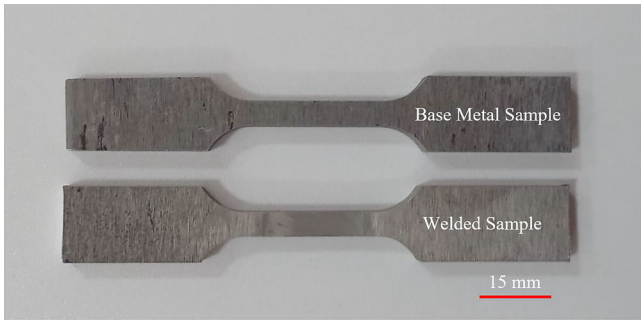

FIGURE 6 Base metal and welded fatigue test specimens.[1] [Colour figure can be viewed at wileyonlinelibrary.com]

4 | RESULTS AND DISCUSSION

4.1 | Tensile test

Tensile test results were taken as a reference to determine the most appropriate welding parameters for fatigue tests. Preliminary experiments were conducted with many different welding parameters. The highest mechanical properties according to tensile strength were obtained at 1250 rpm, 400 mm.min^{-1} welding parameter with a joining efficiency of 88%. In this welding parameter, very similar tensile strength values were obtained from three samples removed from the joined plate. This shows that continuity is achieved throughout the weld seam. The comparison of the stress–strain diagram obtained from the samples joined at this welding parameter with the stress–strain diagram obtained from the base material is shown in Figure 8. It is seen that the welding process also reduces the ductility of the material. Photographs of the samples joined at 1250 rpm, 400 mm.min^{-1} parameter after the tensile test are shown in Figure 9. As a result of tensile testing, fractures occurred in the weld metal.

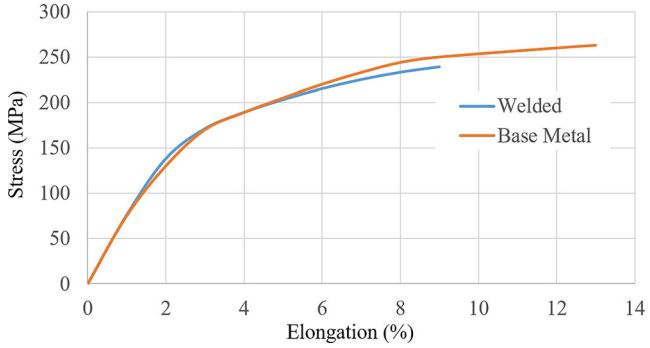

FIGURE 8 Comparison of tensile diagrams of welded samples at 1250 rpm 400 mm.min^{-1} welding parameter and base metal samples.[1] [Colour figure can be viewed at wileyonlinelibrary.com]

FIGURE 7 Microhardness measurement points.[1]

4.2 | Micro–macrostructure

The top surface appearance of the plate joined at 1250 rpm, 400 mm.min^{-1} welding parameter, where 88% joining efficiency was achieved according to tensile strength, is shown in Figure 10A. It can be seen that a smooth weld seam is formed on the upper surface and there is no intense flash formation. The macrostructure photograph of the cross-section of the plate joined at 1250 rpm, 400 mm.min^{-1} welding parameter is shown in Figure 10B. When Figure 10B is examined, at the welding parameter of 1250 rpm, 400 mm.min^{-1} it is seen that joining occurs, and no defects take place at the macro level. Although the SZ is clearly visible, other regions in the macrostructure are not very prominent since a single-phase α-Mg structure is formed in all regions. Additionally, there is a thinning in the cross-section due to the shoulder plunge depth. It is clear that in order for this thinning to be compensated mechanically, the mechanical properties in the weld area where the thinning occurs must be higher than the BM mechanical properties.

Microstructure photographs were taken at two different scales with an optical microscope from the cross-section of the joined plate at 1250 rpm, 400 mm.min^{-1} welding parameter. Microstructure photographs taken from BM, HAZ, TMAZ, and SZ are shown in Figure 11. It is seen that a single-phase α-Mg structure is formed in all regions. It is seen that the grains are smaller in SZ and BM compared to TMAZ and HAZ.

FIGURE 9 Photograph of the samples joined at 1250 rpm 400 mm.min^{-1} parameter after the tensile test.[1] [Colour figure can be viewed at wileyonlinelibrary.com]

4.3 | Microhardness

The microhardness values measured from the cross-section of the joined plate at the welding parameter of 1,250 rpm, 400 mm.min^{-1}, where the highest joining efficiency is achieved, are shown in Figure 12. It is seen that the lowest hardness is obtained in the weld metal center, the hardness is slightly higher in the TMAZ, which is close to the SZ, and the hardness does not change significantly in the HAZ and BM. Generally, when the hardness distribution in the weld cross section is evaluated, no large fluctuations in hardness are detected. It is considered normal that there are no large fluctuations in hardness since the welding process is carried out with low heat input in the FSW process and therefore a single-phase α-Mg structure is formed in all regions.

4.4 | Fatigue test

Low cycle fatigue test results obtained from base metal and welded samples are shown in Figure 13. Low cycle

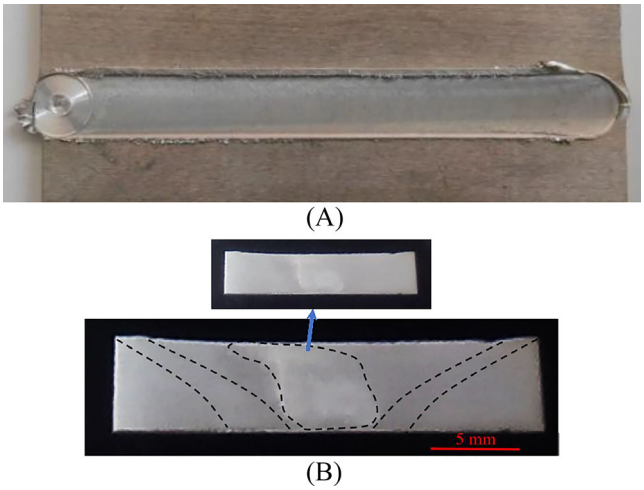

FIGURE 10 Macro view at 1250 rpm, 400 mm.min^{-1} welding parameter. (A) Upper surface view, (B) section view.[1] [Colour figure can be viewed at wileyonlinelibrary.com]

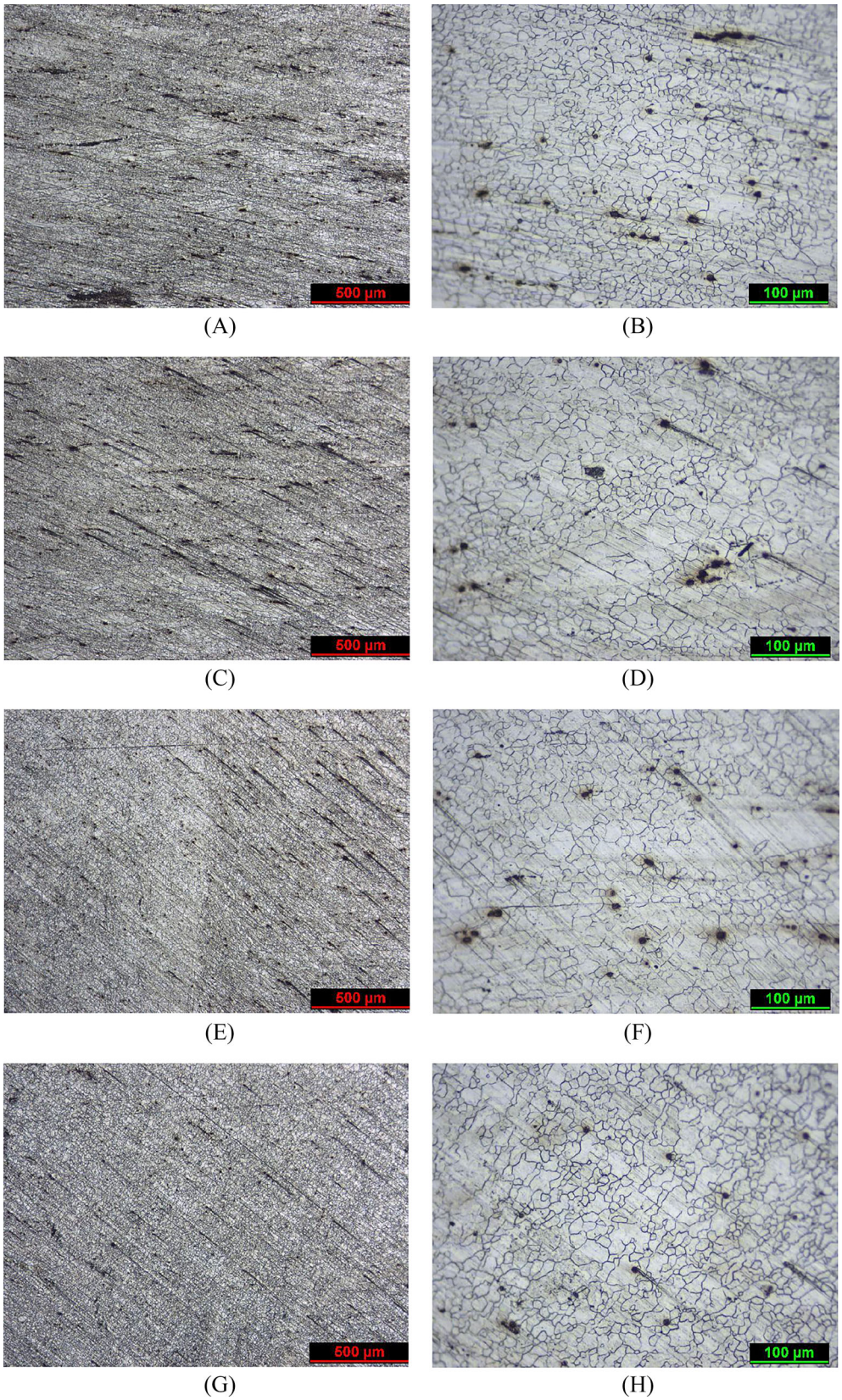

FIGURE 11
Microstructures (A-B) BM, (C-D) HAZ, E-F) TMAZ, G-H) SZ.[1] [Colour figure can be viewed at wileyonlinelibrary.com]

fatigue limit was considered as 50,000 cycles. At 0.2% elongation, all of the base metal and welded samples passed this cycle limit without failure. At an elongation rate of 0.3%, all of the base metal samples exceeded this limit, but it was observed that the welded samples started to fail at this elongation rate. With increasing elongation rate, both base metal and welded samples suffered failure. The number of cycles to failure was very similar for

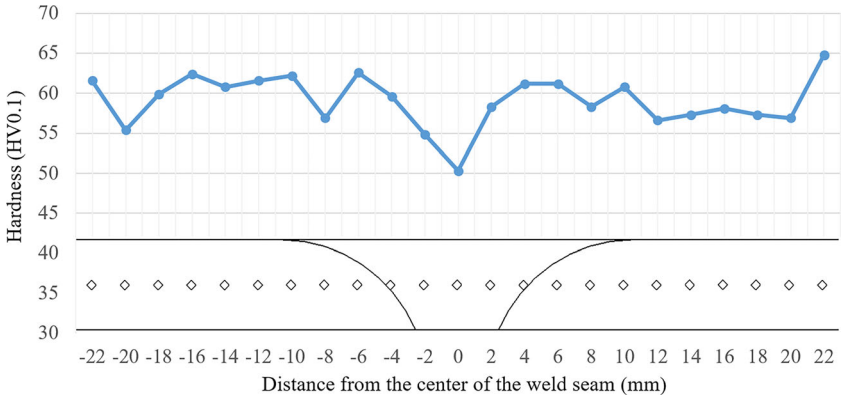

FIGURE 12 Hardness distribution in the weld cross-section.[1] [Colour figure can be viewed at wileyonlinelibrary.com]

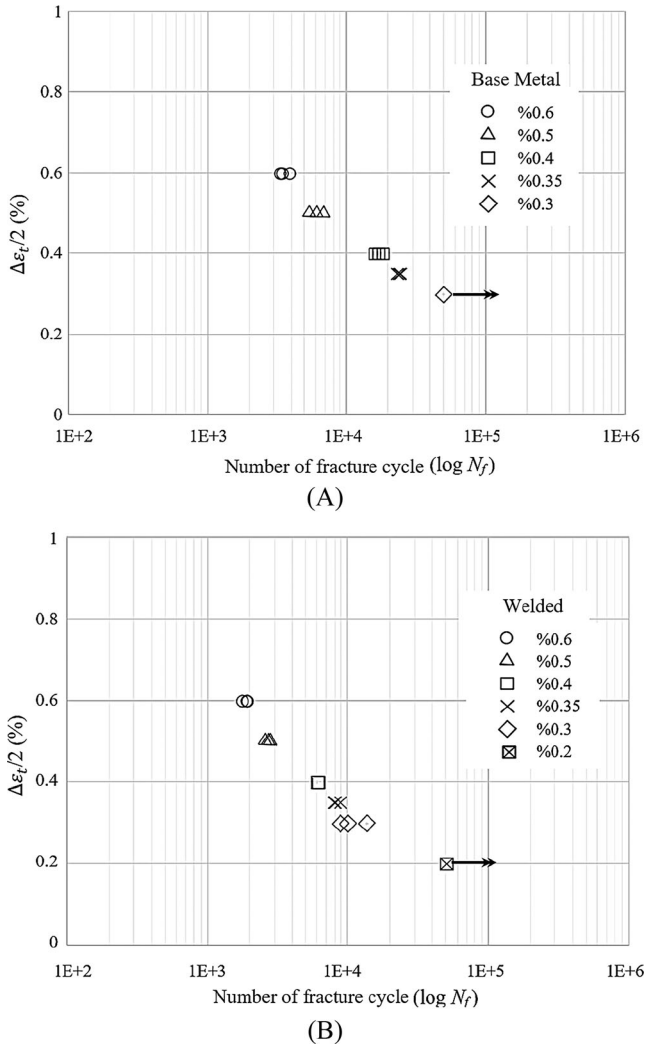

FIGURE 13 Strain controlled low cycle fatigue test results (A) base metal samples, (B) welded samples.[1]

each strain rate in the welded samples. This showed that the weld quality did not change along the weld seam.

Low cycle fatigue test data are represented by the Coffin-Manson equation[48,49]:

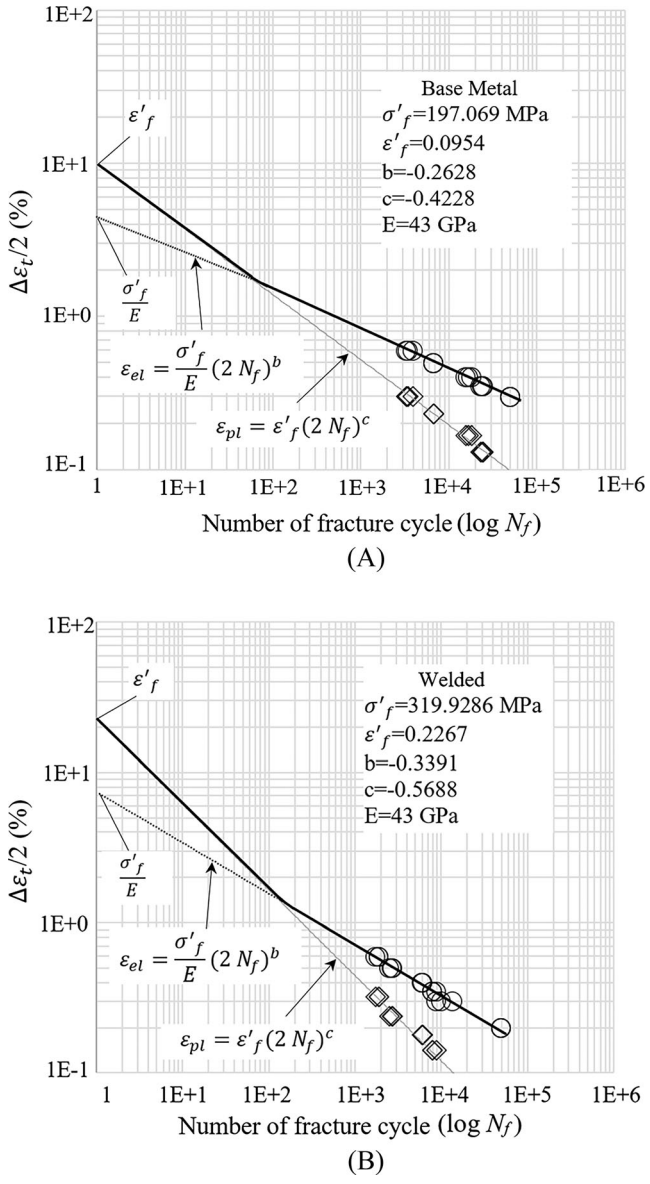

FIGURE 14 Low cycle fatigue parameters according to the Coffin-Manson-Basquin equation (A) base metal samples, (B) welded samples.[1]

$$\varepsilon_a = \frac{\sigma_f'}{E}(2N_f)^b + \varepsilon_f'(2N_f)^c \quad (1)$$

In this equation, σ_f' is the axial fatigue strength coefficient and b is the axial fatigue strength exponent, N_f is the number of fracture cycle. ε_f' and c are the axial fatigue ductility coefficient and axial fatigue ductility exponent, respectively.

Low cycle fatigue parameters of welded and base metal samples were obtained according to the Coffin-Manson-Basquin equation. Figure 14 shows the parameters obtained according to the elastic and plastic elongation ratio. In Figure 14, for each number of fracture cycles, round data defines the elastic strain and rhombic data defines the plastic strain.

4.5 | SEM investigation

The fractured surfaces of the welded test specimens, which were damaged as a result of the fatigue tests, were examined with SEM. As seen in Figure 15, it is seen that fatigue starts from the lower surface of the weld and progresses towards the upper surface. Weld toes are critical areas in the fatigue behavior of welded joints.[50] In the traditional FSW process, the root of the weld is considered to be the critical region for fatigue damage. In practice, a distance of 0.05 mm was allowed between the tool pin and the bottom plate during the welding process to prevent the tool pin from contacting the bottom plate. For this reason, there is a high probability of cold joining occurring in the weld root section due to the nature of the process.

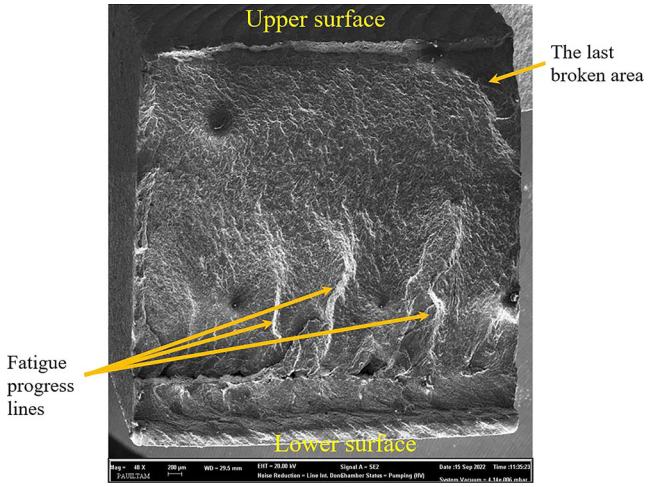

FIGURE 15 Welded fractured surface as a result of fatigue test.[1] [Colour figure can be viewed at wileyonlinelibrary.com]

5 | CONCLUSION

In joining 5.2 mm thick AZ31 magnesium alloy with FSW, a joining efficiency of 88% according to tensile strength has been achieved with a tool with a 21 mm shoulder diameter M5 threaded pin and a pin length of 5 mm, with a welding parameter of 1,250 rpm, 400 mm.min^{-1}. When the micro and macrostructure photograph of the cross-section of the welded plate at 1250 rpm, 400 mm.min^{-1} welding parameter was examined, it was seen that the joining was performed completely, and no defects occurred at the macro level. In the macrostructure, the stirring zone is clearly visible, but since a single-phase α-Mg structure is formed in all regions, other regions are not obvious. In addition, in this parameter, since the single-phase α-Mg structure has formed in all regions of the joined samples, no large fluctuations in hardness have been observed, and this is considered normal since welding has been done with low heat input. According to the low cycle fatigue test results performed on welded and base metal samples, the base metal samples exceeded the 50,000 cycle limit with an elongation rate of 0.3% and the welded samples with an elongation rate of 0.2%. Very similar fatigue test results were obtained from the welded samples for each unit elongation rate, which showed that the weld quality was achieved throughout the seam.

AUTHOR CONTRIBUTIONS

Murat Türkan: Writing—original draft; visualization; validation; software; methodology; investigation; formal analysis; data curation. **Özler Karakaş:** Writing—original draft; visualization; validation; software; methodology; investigation; formal analysis; data curation. **Filippo Berto:** Review and editing; supervision; methodology; conceptualization.

AKNOWLEDGEMENTS

This study was fully supported by the Scientific Research Coordination Unit of Pamukkale University under the following Project Number: 2019FEBE039. Murat Türkan would like to address his special thanks to Prof. Dr. Filippo BERTO for his support during all the duration of his Ph.D. studies.

DATA AVAILABILITY STATEMENT

The data that support the findings of this study are available from the corresponding author upon reasonable request.

ORCID

Filippo Berto https://orcid.org/0000-0001-9676-9970

REFERENCES

1. Türkan M. *The numerical analysis and the investigation of low cycle fatigue behavior of magnesium alloys joined by friction stir welding*. Pamukkale University, Institute of Science, Mechanical Engineering, Ph.D. Thesis; 2022.
2. Sahoo M, Thomas-Sadowski S. *American foundry society*. Design, Products & Applications; 2011.
3. Moosbrugger C (Ed). *Introduction to magnesium alloys*. ASM International; 2017.
4. Prasad SVS, Prasad SB, Verma K, Mishra RK, Kumar V, Singh S. The role and significance of magnesium in modern day research-a review. *J Magnes Alloys*. 2022;10(1):1-61. doi:10.1016/j.jma.2021.05.012
5. Monteiro WA (Ed). *Special issues on magnesium alloys*. Rijeka; 2011.
6. Kulekci MK. Magnesium and its alloys applications in automotive industry. *Int J Adv Manuf Technol*. 2008;39(9-10):851-865. doi:10.1007/s00170-007-1279-2
7. Ullmann M, Kittner K, Henseler T, Stöcker A, Prahl U, Kawalla R. Development of new alloy systems and innovative processing technologies for the production of magnesium flat products with excellent property profile. *Procedia Manuf*. 2019;27:203-208. doi:10.1016/j.promfg.2018.12.065
8. Kierzek A, Adamiec J. Evaluation of susceptibility to hot cracking of magnesium alloy joints in variable stiffness condition. *Arch Metall Mater*. 2011;56(3):759-767. doi:10.2478/v10172-011-0084-y
9. Kiełbus A. Microstructure and Properties of Casting Magnesium Alloys Designed to Work in Elevated Temperature. In: Tański T, Borek W, Król M, eds. *Magnesium alloys - selected issue*. In, IntechOpen; 2018.
10. Johari NA, Alias J, Zanurin A, Mohamed NS, Alang NA, Zain MZM. Recent progress of self-healing coatings for magnesium alloys protection. *J Coat Technol Res*. 2022;19(3):757-774. doi:10.1007/s11998-021-00599-2
11. Loukil N. Alloying Elements of Magnesium Alloys: A Literature Review. In: Tański T, Jarka P, eds. *Magnesium alloys structure and properties*. IntechOpen; 2022.
12. Padmanaban G, Balasubramanian V. An experimental investigation on friction stir welding of AZ31B magnesium alloy. *Int J Adv Manuf Technol*. 2010;49(1-4):111-121. doi:10.1007/s00170-009-2368-1
13. Padmanaban G, Balasubramanian V, Sarin Sundar JK. Influences of welding processes on microstructure, hardness, and tensile properties of AZ31B magnesium alloy. *J Mater Eng Perform*. 2010;19(2):155-165. doi:10.1007/s11665-009-9389-7
14. Mirza FA, Chen DL. *Fatigue of magnesium alloys*. Aerospace Materials Handbook; 2013.
15. Cao X, Jahazi M, Immarigeon JP, Wallace W. A review of laser welding techniques for magnesium alloys. *J Mater Process Technol*. 2006;171(2):188-204. doi:10.1016/j.jmatprotec.2005.06.068
16. Czerwinski F. Welding and joining of magnesium alloys. In: *Magnesium alloys, magnesium alloys-design, processing and properties*. IntechOpen; 2011:469-490.
17. Templeman Y, Ben Hamu G, Meshi L. Friction stir welded AM50 and AZ31 mg alloys: microstructural evolution and improved corrosion resistance. *Mater Charact*. 2017;126:86-95. doi:10.1016/j.matchar.2017.02.018
18. Asadi P, Kazemi-Choobi K, Elhami A. Welding of Magnesium Alloys. In: Monteiro WA, ed. *New features on magnesium alloys*. InTech; 2012.
19. Ugender S. Influence of tool pin profile and rotational speed on the formation of friction stir welding zone in AZ31 magnesium alloy. *J Magnes Alloys*. 2018;6(2):205-213. doi:10.1016/j.jma.2018.05.001
20. Yang J, Ni DR, Wang D, Xiao BL, Ma ZY. Strain-controlled low-cycle fatigue behavior of friction stir-welded AZ31 magnesium alloy. *Metall and Mat Trans a*. 2014;45(4):2101-2115. doi:10.1007/s11661-013-2129-5
21. Sun DX, Sun DQ, Gu XY, Xuan ZZ. Hot cracking of metal inert gas arc welded magnesium alloy AZ91D. *ISIJ Int*. 2009;49(2):270-274. doi:10.2355/isijinternational.49.270
22. Luo H, Hao C, Zhang J, Gan Z, Chen H, Zhang H. Characteristics of resistance welding magnesium alloys AZ31 and AZ91. *Weld J*. 2011;90:249-257.
23. Meng X, Huang Y, Cao J, Shen J, dos Santos JF. Recent progress on control strategies for inherent issues in friction stir welding. *Prog Mater Sci*. 2021;115:100706. doi:10.1016/j.pmatsci.2020.100706
24. Mishra RS, Ma ZY. Friction stir welding and processing. *Mater Sci Eng: R: Reports*. 2005;50(1-2):1-78. doi:10.1016/j.mser.2005.07.001
25. Thomas WM. Friction stir butt welding. Int Patent Appl No. PCT/GB92/02203. 1991.
26. Kumar SD, Kumar SS. Effect of heat treatment conditions on ballistic behaviour of various zones of friction stir welded magnesium alloy joints. *Trans Nonferrous Met Soc Chin*. 2021;31(1):156-166.
27. Turkan M, Karakas Ö. Two different finite element models investigation of the plunge stage in joining AZ31B magnesium alloy with friction stir welding. *SN Appl Sci*. 2021;3(2):165.
28. Türkan M, Karakaş Ö. Numerical modeling of defect formation in friction stir welding. *Mater Today Commun*. 2022;31:103539. doi:10.1016/j.mtcomm.2022.103539
29. MohdA W, Khan ZA, Siddiquee AN. Review on underwater friction stir welding: a variant of friction stir welding with great potential of improving joint properties. *Trans Nonferrous Met Soc Chin*. 2018;28(2):193-219.
30. Razal Rose A, Manisekar K, Balasubramanian V. Effect of axial force on microstructure and tensile properties of friction stir welded AZ61A magnesium alloy. *Trans Nonferrous Met Soc Chin*. 2011;21(5):974-984. doi:10.1016/S1003-6326(11)60809-1
31. Türkan M, Karakaş Ö. The effect of welding defects to thetensile behavior in corrosive environmentof AISI 304L stainless steel joined withshielded metal electrode. *J Achiev Mater Manuf Eng*. 2017;1(85):26-30.
32. Karakas Ö, Morgenstern C, Sonsino C M, Hanselka H, Vogt M, Dilger, K. Grundlagen für die praktische Anwendung des Kerbspannungskonzeptes zur Schwingfestigkeitsbewertung von geschweißten Bauteilen aus Magnesiumknetlegierungen. Fraunhofer-Institute for Structural Durability and System Reliability (LBF), Darmstadt, Report No. FB-232; 2007. Institute for Welding (ifs), Braunschweig, Report-No 17; 2007.
33. Marsavina L, Iacoviello F, Dan Pirvulescu L, Di Cocco V, Rusu L. Engineering prediction of fatigue strength for AM50 magnesium alloys. *Int J Fatigue*. 2019;127:10-15. doi:10.1016/j.ijfatigue.2019.05.028

34. Chauhan AB, Kumar SA. Effect of friction stir welding parameters on impact strength of the AZ31 magnesium alloy joints. *Int J Mech Prod Eng Res Dev*. 2018;8(2):615-622.
35. Rajakumar S, Razalrose A, Balasubramanian V. Friction stir welding of AZ61A magnesium alloy: a parametric study. *Int J Adv Manuf Technol*. 2013;68(1-4):277-292.
36. Patel N, Bhatt KD, Mehta V. Influence of tool pin profile and welding parameter on tensile strength of magnesium alloy AZ91 during FSW. *Procedia Technol*. 2016;23:558-565. doi:10.1016/j.protcy.2016.03.063
37. Singh B, Singh K, Sahni V. Mechanical and metallurgical properties of friction stir welded magnesium alloy joints using different pin profiles. *Int J Mech Prod Eng*. 2018;6:8.
38. Singh RP, Dubey S, Singh A, Kumar S. A review paper on friction stir welding process. *Mater Today: Proc*. 2021;38:6-11.
39. Dayananda Sagar College of Engineering, John J, Shanmughanatan SP, Kiran M. Friction stir welding of wrought Aluminium alloys - a short review. *Int J Eng Trends Technol*. 2016;32(2):76-81.
40. Zhang YN, Cao X, Larose S, Wanjara P. Review of tools for friction stir welding and processing. *Can Metall Quart*. 2012;51(3):250-261.
41. Long L, Chen G, Zhang S, Liu T, Shi Q. Finite-element analysis of the tool tilt angle effect on the formation of friction stir welds. *J Manuf Process*. 2017;30:562-569. doi:10.1016/j.jmapro.2017.10.023
42. Vigneshkumar M, Padmanaban G, Balasubramanian V. Influence of tool tilt angle on the formation of friction stir processing zone in cast magnesium alloy ZK60/SiCp surface composites. *Metallogr Microstruct Anal*. 2019;8(1):58-66. doi:10.1007/s13632-018-0507-5
43. Sun S-J, Kim J-S, Lee WG, Lim J-Y, Go Y, Kim YM. Influence of friction stir welding on mechanical properties of butt joints of AZ61 magnesium alloy. *Adv Mater Sci Eng*. 2017;2017:1-13.
44. Ugender S, Kumar A, Reddy AS. Microstructure and mechanical properties of AZ31B magnesium alloy by friction stir welding. *Procedia Mater Sci*. 2014;6:1600-1609. doi:10.1016/j.mspro.2014.07.143
45. Goel S, Naveen G, Gupta A, Gulati P. Effect of process parameters on mechanical and metallurgical properties of friction stir processed AZ31Mg alloy. *Mater Today: Proc*. 2018;5:4575-4583.
46. Sahu PK, Pal S. Effect of shoulder diameter and plunging depth on mechanical properties and thermal history of friction stir welded magnesium alloy. In: 5th Int. 26th All India Manuf. Technol. Des. Res. Conf. (AIMTDR 2014). 2014; 12–17.
47. Sahu PK, Pal S. Effect of FSW parameters on microstructure and mechanical properties of AM20 welds. *Mater Manuf Process*. 2018;33(3):288-298.
48. Albinmousa J. Fatigue of Magnesium-Based Materials. In: Gupta M, ed. *Magnesium - the wonder element for engineering/biomedical applications*. IntechOpen; 2020.
49. Karakas Ö, Gülsöz A, Kaufmann H, Sonsino CM. Fatigue behaviour of welded joints from magnesium alloy (AZ31) according to the local strain concept. *Materialwissenschaft Werkst*. 2010;41(2):73-82. doi:10.1002/mawe.200900543
50. Karakas Ö. Consideration of mean-stress effects on fatigue life of welded magnesium joints by the application of the smith–Watson–topper and reference radius concepts. *Int J Fatigue*. 2013;49:1-17. doi:10.1016/j.ijfatigue.2012.11.007

How to cite this article: Türkan M, Karakaş Ö, Berto F. Low cycle fatigue behavior of AZ31 magnesium alloy joined by friction stir welding. *Fatigue Fract Eng Mater Struct*. 2024;47(11):4165-4175. doi:10.1111/ffe.14411